23

Extraction of Estuarine/Coastal Environmental Bodies from Satellite Data through Image Segmentation Techniques

Ana Teodoro and Hernâni Gonçalves
Geo-Space Sciences Research Centre - Faculdade de Ciências, Universidade do Porto
Portugal

1. Introduction

The analysis of satellite imagery of natural scenes presents many unique problems, and it differs from the analysis and segmentation of urban, commercial, or agricultural areas. Natural scenes are not structured and cannot be represented easily by regular rules or grammars. The appearance of natural objects can vary greatly based on the geographic area, the season, the current weather conditions, or the past weather conditions (Soh & Tsatsoulis, 1999).

Segmentation is defined as the process that partitions an image into regions that are homogeneous according to given criteria (Gonzalez & Woods, 2008). Image segmentation is typically used to locate objects and identify boundaries. A number of problems in remote sensing require the segmentation of natural spectral classes such as water bodies, clouds or forested areas (Lira, 2006).

A wide variety of image segmentation methods may be found in the literature (Cheng et al., 2001; Pal & Pal, 1993). The most popular techniques are those based on gray level thresholding, including global thresholding (e.g. Otsu's method) or using local information (e.g. co-occurrence matrix). Another class of methods comprise segmentation obtained through the detection of edges, including those based on parallel differential operators (e.g. Sobel gradient) and the Canny's method (Canny, 1986). There are also methods that are based on finding the regions directly on the image domain (pixel values), where the region growing and region split-and-merge approaches are some of the available procedures (Gonzalez & Woods, 2008). The segmentation using morphological watershed is another approach, based on the feature space (the watershed transform of the image), and it is particularly attractive because it combine positive attributes of the methods previous referred (Gonzalez & Woods, 2008).

The coastal areas are zones of primary importance from human and ecological points of view. More than half of the world population lives at less than 100 km from a coast, which express the importance of coastal areas from the human point of view. The same occurs from the ecological point of view, since coastal zones are areas of strong interactions between the biosphere, atmosphere, and hydrosphere. An estuary is a partially enclosed body of water, where freshwater from rivers and streams flows into the oceans, mixing with the seawater. Estuaries and the lands surrounding them are places of transition from land to

sea, and from fresh to saltwater. Estuarine outflow plumes are important coastal processes whose variable nature can make it difficult to monitor using traditional ship-based surveys. Plumes are a mixture of fresh water and river sediment load, with some dilution caused by currents. The river plumes are turbid and carry a high load of suspended sediments. Since these suspended sediments can be associated with nutrients, pollutants and other materials, it is of crucial importance to remotely survey their dispersal in order to assess the environmental quality of the regions surrounding river mouths.

The main idea of this chapter is to describe and evaluate different segmentation methods, in order to accurately extract two different estuarine/coastal features: river plumes and sand spits.

Several studies typically use a threshold value for determining the plume boundaries (e.g. Otero & Siegel, 2004). Dzwonkowski & Yan (2005) employed a gradient approach (MODIS and SeaWiFS data) on account of previous observations of physical differences (e.g. salinity) between the estuarine outflow and the ambient water. Valente & Silva (2009) used three years of MODIS-Aqua normalized water-leaving radiance to study Tagus estuary turbid plume. In the previous examples, the turbid plume was detected only by the backscattering characteristics of the surface waters in the vicinity of the estuary mouth. Nezlin et al. (2005) used SeaWiFS images to analyze the spatial-temporal dynamics of plumes in the San Pedro Shelf (California) and identified the factors that influence the incidence and dispersal patterns of plumes. Lira et al. (1997) developed a methodology to characterize the spatial distribution of suspended sediments in Pánuco river plume (Gulf of Mexico) employing remote sensing and pattern recognition techniques. Several attempts to segment specific spectral classes, as open water bodies, have been reported in the literature (Lira, 2006; McFeeters, 1996; Daya-Sabar et al., 1995).

A spit is a ridge or embankment of sediments attached to the land at one end, with the other ending in open waters, being younger than the land to which it is attached. The body of the spit extends from the land outward for some distance above the water. The size and shape of recurves depends on the space available on the inner side of a growing spit (Bird, 2008). The evolution of many spits has been modified by the addition of artificial structures. Sand spits are ecosystems of great biological interest. Therefore, environmental monitoring using remote sensing data and image processing algorithms is essential for assessing the local changes in this area.

A water body is a region (or area) limited by a well-defined topographic boundary. A sand spit does not present a well-defined topographic boundary. Moreover, the boundary is not static in time, as the majority of the water bodies. Therefore, the extraction of a sand feature from a water environment (e.g. an estuary) is a complex task and the segmentation techniques developed should be different in several aspects that those applied and optimized for the river plumes extraction.

This chapter aims to address the problem of segmentation of water bodies and sandy bodies in an estuarine/coastal environment, in order to accurately extract them through satellite data, allowing for further boundaries delineation. Different segmentation algorithms were applied and developed/optimized in order to correctly determine the features boundaries and accurately estimate the river plume size and sand spit area. Although the only considered attribute as output was the dimension, other attributes may be obtained from the segmentation result. The use of different types of satellite data (raw images and satellite products) is also a challenge and an important contribution of this work.

2. Methodology

The selection of the segmentation approach used to extract an estuarine/coastal environmental body, from remote sensing images, should account for the type of feature to be extracted. A flowchart which illustrates the proposed approaches is provided in Fig. 1. A concise characterization of the study area and the satellite data used in this work is given in section 2.1 and corresponding subsections. The procedures applied for the extraction of river plumes and sand spits dimensions are briefly described in the section 2.2 and section 2.3, respectively.

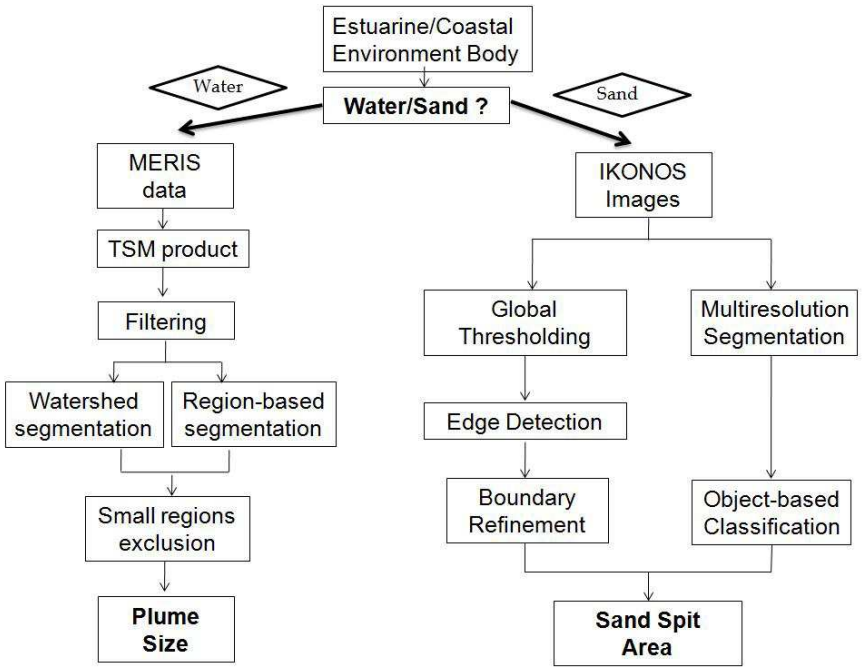

Fig. 1. Flowchart of the developed segmentation approaches for the extraction of river plumes and sand spits.

2.1 Study area and satellite data

The study area chosen in this work was the Douro River Estuary (Fig. 2). Douro is a granitic drowned valley river (927 km), draining to the N-W shore of Portugal. The Douro river basin is the largest hydrographical basin in the Iberian Peninsula (97,682 km^2). Its estuary is located in the Western Portuguese coast, subject to the North Atlantic meteorological and hydrodynamic conditions.

Two thirds of the river mouth are protected by a very dynamic sand spit (Cabedelo), creating a micro-ecosystem of great biological interest. Cabedelo sand spit is a very dynamic morphologic structure. This sand spit has an average length of 800 m, an average width of 300 m and an area that usually range between 220 000 and 270 000 m^2. The Cabedelo acts as a barrier, protecting the estuary banks from waves, especially during storms. In the last

decades, the protection function of the sand spit has been reduced, especially due to the retreatment to the interior of the estuary. Therefore, two breakwaters were constructed (between 2004 and 2007) to stabilize the river mouth.

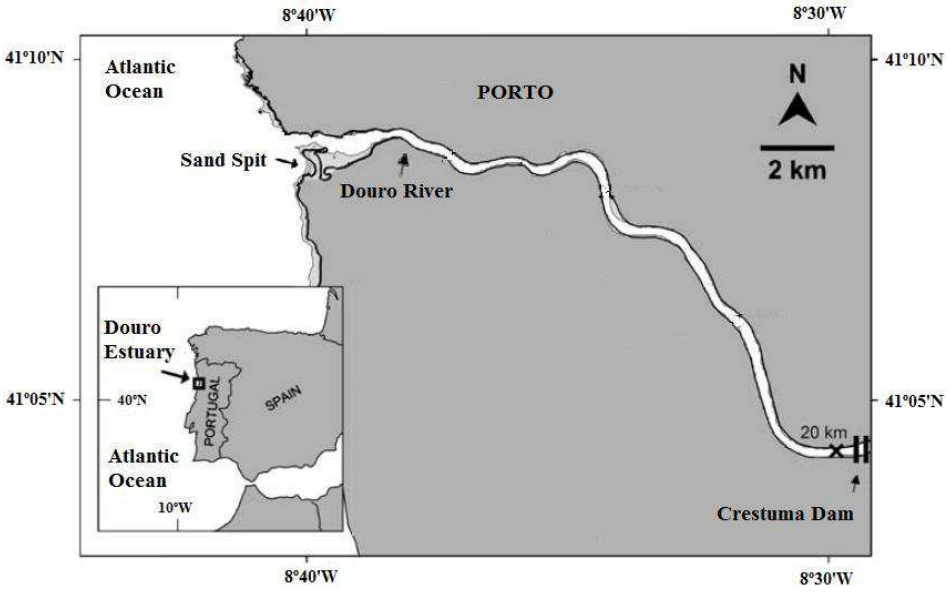

Fig. 2. Study area location in the Portuguese west coast (adapted from Portela (2008))

As previously mentioned and illustrated in Fig. 1, the considered type of satellite data depends on the features to be extracted. Accordingly, MERIS data and IKONOS-2 images are briefly addressed in the following (2.1.1 and 2.1.2, respectively).

2.1.1 MERIS data

In mid-2002 the European Space Agency (ESA) launched the MERIS (MEdium Resolution Imaging Spectrometer) hosting satellite ENVISAT. MERIS is an imaging spectrometer that measures the solar radiation reflected by the Earth, at a ground spatial resolution of 300 m, in 15 spectral bands (390 - 1040 nm), programmable in width and position, in the visible and near infrared. The primary mission of MERIS is the measurement of sea color in oceans and coastal areas. Knowledge of the sea color can be converted, for instance, into a measurement of total suspended matter (TSM) concentration. The algorithm of the ground segment of MERIS, used to retrieve the TSM concentration from spectra of radiances and reflectance of coastal waters, is an inverse modeling technique, carried out by an artificial neural network (Doerffer et al., 1999; Schiller & Doerffer, 2005). The TSM concentration is expressed as a concentration in g/m^3 or Log10 (g/m^3) with a valid range between 0.01-50.00 g/m^3.

The particulate backscatter at 442 nm is deduced from the water-leaving reflectance spectrum and converted from optical units (backscatter in m^{-1}) to geophysical units (concentration in g/m^3), using a fixed conversion factor (equation 1), derived for measurements on water samples using a GF/F filter. The TSM concentration for all the scenes is given by the following equation (1):

$$Log_{10}(TSM)=Scale*DV+Offset \quad (1)$$

where DV is the digital value (no physical significance) for each pixel, the scale value is 0.015748031437397003 and the offset value is -2.01574802398681 (European Space Agency, 2007). The TSM concentration retrieved from one MERIS scene considered in this study is illustrated in Fig. 3.

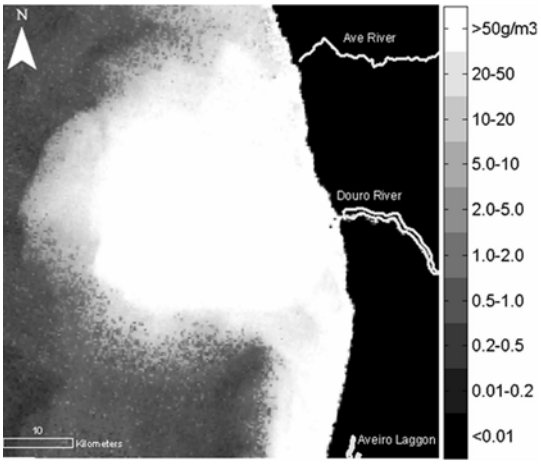

Fig. 3. TSM concentration retrieved from one of the considered MERIS scenes (08/03/2003).

In this study, a first dataset (assigned hereafter as "Dataset A") composed by 21 MERIS Full Resolution scenes (level 2 data) from March 2003 to January 2005 was considered (data provided by ESA), after the rejection of MERIS scenes that present: more than 10% cloud cover or invalid TSM quality flag; errors in the acquisition process (data corruption); or incoherent related river flow data. The number of scenes in each individual month is highly variable, from zero (e.g. August 2003) to 4 (June 2003). The most represented months in the considered three years (2003-2005) are May, June and September. Concerning the year distribution, the coverage in 2003 and 2004 was almost uniform, but in 2005 only one scene was available (Teodoro et al., 2008).

In the work developed by Teodoro et al. (2009), it was suggested that the accuracy could be improved by increasing the dataset. Additionally, a complete seasonal study of the Douro river plume would be interesting, for which a one year window of MERIS data is required. Therefore, a project was submitted to ESA in order to acquire a one year window (one hydrologic year) of MERIS data. A total of 107 MERIS scenes were considered, between August 2008 and October 2009 ("Dataset B"). No previous selection was performed. All the MERIS scenes available for this period were considered. The future data exclusion criteria will be based in the atmospheric conditions and in problems associated to the segmentation stage, as described in the section 4.1.2. Due to the fact that breakwaters were constructed between March 2004-2007 in the study area, these two datasets (A and B) were analyzed separately.

2.1.2 IKONOS-2 images

As already referred, one of the main objectives of this study was to extract the boundaries between Douro river and Cabedelo sand spit, and consequently estimate the sand spit area.

Therefore, the use of high spatial resolution satellite data is required. Six IKONOS-2 images were used in this study, acquired between 2001 and 2007, under the scope of the ESA project Earth Observation Program, Category 1 (ID#5899). IKONOS-2 is able to collect black-and-white (panchromatic) images with approximately 1-meter resolution and multispectral imagery with 4-meter resolution. The IKONOS-2 orbit altitude is approximately 681 km and inclined 98.1º to the equator, providing sun-synchronous operation. The main IKONOS-2 data specifications are given in Table 1.

Band	Spectral Range (μm)	Spatial resolution (m)	Swath width (km)
Panchromatic	0.45-0.90	1	11.3
Band 1 (blue)	0.45-0.53	4	
Band 2 (green)	0.52-0.61		
Band 3 (red)	0.64-0.72		
Band 4 (near infrared)	0.77-0.88		

Table 1. IKONOS- 2 data specifications: spectral range, spatial resolution and swath width.

The data were full 11-bit radiometric resolution and were geo-referenced to the Universal Transverse Mercator (UTM) coordinate system, Zone 29 North, World Geodetic System 1984 (WGS84). Information about the time of acquisition, cloud cover, sun angle elevation and nominal collection elevation, is given in Table 2.

Date (yyyy/mm/dd)	Acquisition time (GMT)	Cloud cover (%)	Sun angle Elevation (º)	Nominal collection elevation (º)
2001/12/24	11:44	0	24.54	69.58
2004/06/03	11:43	0	68.66	72.90
2004/07/31	11:55	6	64.61	61.97
2005/06/03	11:39	0	68.36	84.51
2005/09/18	11:36	0	49.01	71.7
2007/06/06	11:39	0	68.42	78.56

Table 2. Information related to the 6 IKONOS-2 images: date and time of acquisition, cloud cover, sun angle elevation and nominal collection elevation.

According to Helder et al., (2003), it appears to be a relationship between satellite elevation angle and geometric accuracy. It was found that higher elevation angles tend to result in lower root mean square error (RMSE). The relationship suggests that satellite elevation angles above 75° tend to maximize the geometric accuracy of the IKONOS-2 product. Terrain correction, even for a relatively 'flat' site (as the sand spit), improved RMSE values at lower satellite elevation angles (Helder et al., 2003). Since the nominal collection elevation values are mostly near or above 75º, there was no need to perform any terrain correction.

2.2 River plumes

As referred before, the MERIS product used in this research provides a suspended sediments concentration image, which allows for the extraction of objects corresponding to river plumes. A saturation of the TSM concentration values (50 g/m^3) is verified for most of

the MERIS scenes, in the coastal waters (Case 2 waters). Figure 3 provides a selected window from MERIS data where the Douro river plume is visible. The proposed segmentation approach for the extraction of river plumes is based on an initial filtering, followed by one of the two addressed segmentation methods: region-based and watershed. The methodology will be briefly described in the following, and further details may be found in (Teodoro et al., 2009).

2.2.1 Initial filtering and segmentation

An initial filtering step is required in order to avoid noise and to smooth the image (and consequently the plume), which is based on a median filter with a 10x10 pixel window. The next and crucial step of the methodology is the segmentation stage. Two different segmentation methods were applied: watershed segmentation using gradients and region-based (region growing) segmentation.

2.2.1.1 Region-based segmentation

Region-based methods assume that neighboring pixels within the same region should have similar values, e.g. intensity, color and texture (Tremeau & Bolel, 1997; Hojjatoleslami & Kittler, 1998). Region growing is a procedure that groups pixels or subregions into larger regions based on predefined criteria for growth. The basic approach is to start with a set of "seed" points, and these regions grow by appending to each seed those neighboring pixels that have predefined properties similiar to the seed (specific ranges of intensity or color). The selection of similarity criteria depends not only on the problem under consideration, but also on the type of image data available (e.g. color, texture). The stopping criteria for this procedure is when no more pixels satisfy the criteria for inclusion in that region. Additional criteria that increase the power of region growing algorithm utilize the concept of size and the shape of the region being grown (Gonzalez & Woods, 2008).

2.2.1.2 Watershed-based segmentation

The major idea of watershed segmentation is based on the concept of topographic representation of image intensity. The gradient magnitude of an image is considered as a topographic surface for the watershed transformation. Watershed segmentation also embodies other principal image segmentation methods including discontinuity detection, thresholding and region processing (Gonzalez & Woods, 2008). Because of these factors, watershed segmentation displays more effectiveness and stableness than other segmentation algorithms. As already referred, the basic concept of watershed is based on visualizing a gray level image into its topographic representation, which includes three basic notions: minima, catchment basins and watershed lines. The objective of watershed segmentation is to find all of the watershed lines (the highest gray level). The most intuitive way to explain watershed segmentation is the *Immersion Approach* (Chen et al., 2004). An efficient algorithm to implement this approach proposed by Vincent & Soille (1991) involves two steps: the first one is called "sorting step" and the other is called "flooding step". Watershed segmentation produces good results for gray level images with different minima and catchment basins. For binary images, however, there are only two gray levels 0 and 1 standing for black and white. If two black blobs are connected together in a binary image, only one minimum and catchment basin will be formed in the topographic surface. The direct application of the watershed segmentation algorithm generally leads to over-segmentation of an image due to noise and other local irregularities of the gradient.

Therefore, it is recommended to smooth the image before starting the watershed segmentation, which is performed through the initial filtering step previously described.

2.2.2 Comparison of the region-based and watershed-based methods

The considered segmentation methods differ in the sense that region-based segmentation is based on the image domain (pixel values), whereas watershed segmentation is based on the feature space (the watershed transform of the image). An example of a segmentation result using these two approaches for the same MERIS scene is given in Fig. 4.

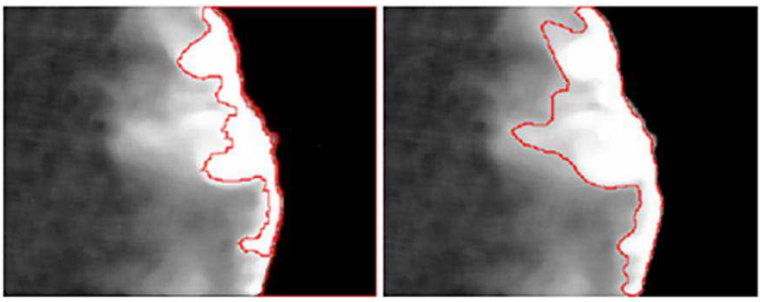

Fig. 4. Plume identification using image segmentation: watershed using gradients obtained through Sobel operator (left); region-based segmentation using a seed value of 225 and a threshold of 30 (right).

Although the segmentation results obtained from the application of these two approaches is different, they should be (linearly) related in some manner, since the segmentation is related to the same object. Fig. 5 illustrates a linear dependence between these two approaches,

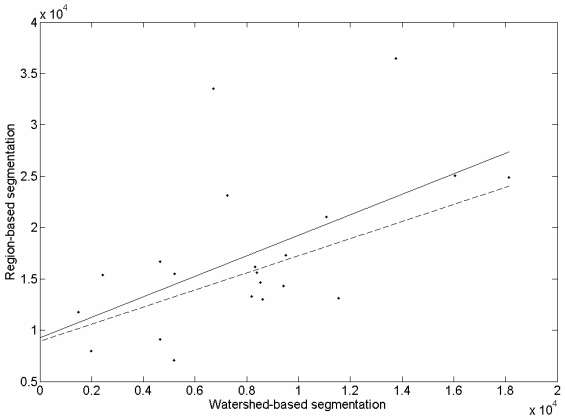

Fig. 5. Scatterplot of the region- and watershed-based segmentation values presented in Table 3. The solid regression line is defined as y=9241.77+1.00x (r=0.57 with p-value=0.007), and is associated to the 21 points. The dashed regression line is defined as y=8930.85+0.83x (r=0.71 with p-value=0.001), and is associated to the remaining 19 points obtained after excluding the two higher values of region-based segmentation (images of 18-06-2003 and 14-05-2003).

supported by a positive and significant correlation of 0.71 between them, where the slope of the regression line is 0.83. This reinforces that, although the shape of the plume is different when using these two segmentation approaches, they produce similar plume sizes related by a scale ratio (0.83 in this example).
This procedure of extracting the river plume object through image segmentation techniques has important practical applications. For instance, the reduction of the river sediment supply may be one of the main causes of the erosion process that has been affecting the Portuguese Northwest coast. The relationship between the river plume size and Cabedelo sand spit area is another challenge of this analysis.

2.3 Sand spits

Two segmentation approaches are addressed for the extraction of sand spits from high spatial resolution images, which are different from those previously described for river plumes extraction. The first is a new proposed methodology and is based on global thresholding refined through detected edges, whereas the second approach consists in a multiresolution segmentation (object-based). The segmentation approaches are applicable to a single band image, for which the NIR or panchromatic bands of the IKONOS-2 images are the most adequate. The NIR is the spectral band which provides better contrast between water and land, whereas the panchromatic band has the advantage of providing a better spatial resolution, and consequently a more accurate delineation of the sand spit. Several aspects regarding the application of these techniques should be taken into account, which are addressed in detail in the following.

2.3.1 Global thesholding refined through detected edges

The proposed approach for the extraction of sand spits is a new methodology, which presents considerable potential for later automation in the future. It consists on histogram global thresholding of the original image through the Otsu method (Otsu, 1979), followed by a refinement through detected edges. Different approaches for edge detection were tested and are addressed in the following.

2.3.1.1 Global thresholding

The histograms of IKONOS-2 images, representing a sand spit and a small neighborhood, are typically associated to a mode on a histogram with bimodal distribution (an example is illustrated in Fig. 6a and Fig. 6b). The Otsu's method is a nonparametric and unsupervised method of automatic threshold selection for image segmentation, having particular importance under the scope of bimodal histograms (Otsu, 1979). It assumes that only the gray-level histogram of the image is available, without other a priori knowledge, allowing for an unsupervised segmentation of an image. It is based on dichotomizing the pixels of the image, transforming the original image to a binary image. The determination of the optimal threshold k^* is performed through an approach based on probabilities computation. It is followed by the computation of discriminant criterion measures (or measures of class separability), generally consisting on finding the gray level k^* for which a discriminant function $\eta(k)$ corresponds to its maximum. It is equivalent to maximize the separability of the resultant classes in the binary image. This method is widely known, and further details may be found in (Otsu, 1979). An example of global thresholding is illustrated in Fig. 7a, regarding the image in Fig. 6a.

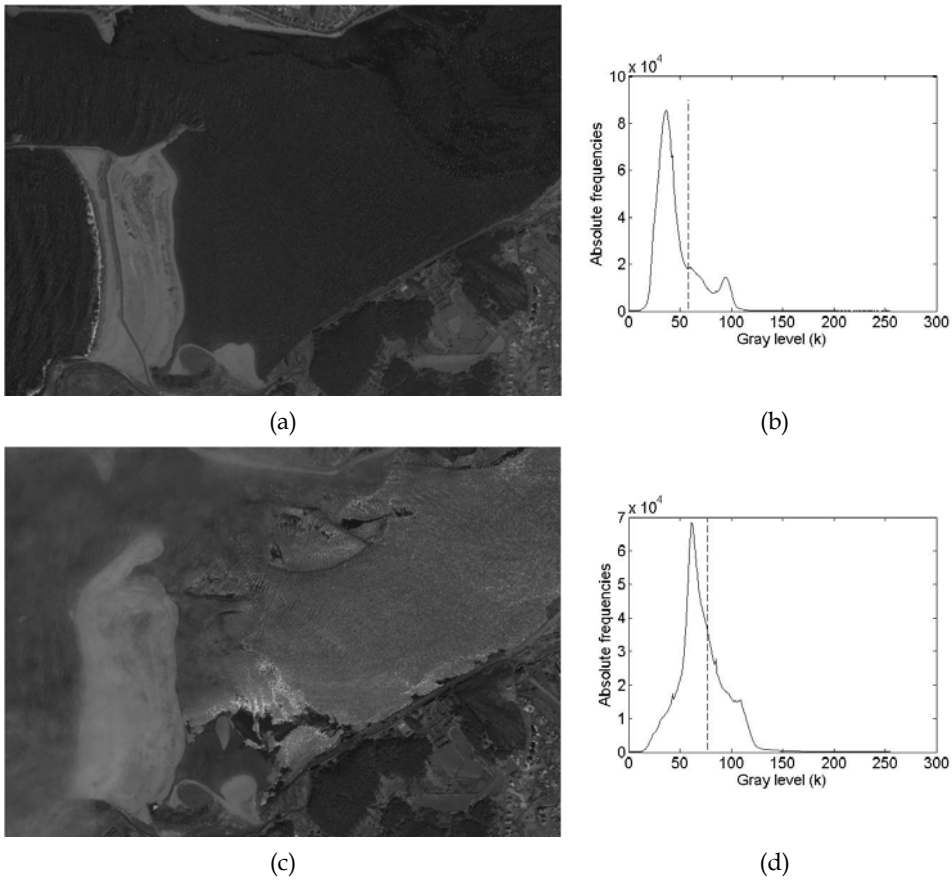

Fig. 6. (a) Panchromatic band of the IKONOS-2 image from 2005/06/03; (b) Histogram of the image in (a), with k*= 58 and $\eta(k^*)$= 0.735; (c) Panchromatic band of the IKONOS-2 image from 2004/06/03; (d) Histogram of the image in (c), with k*= 77 and $\eta(k^*)$= 0.605.

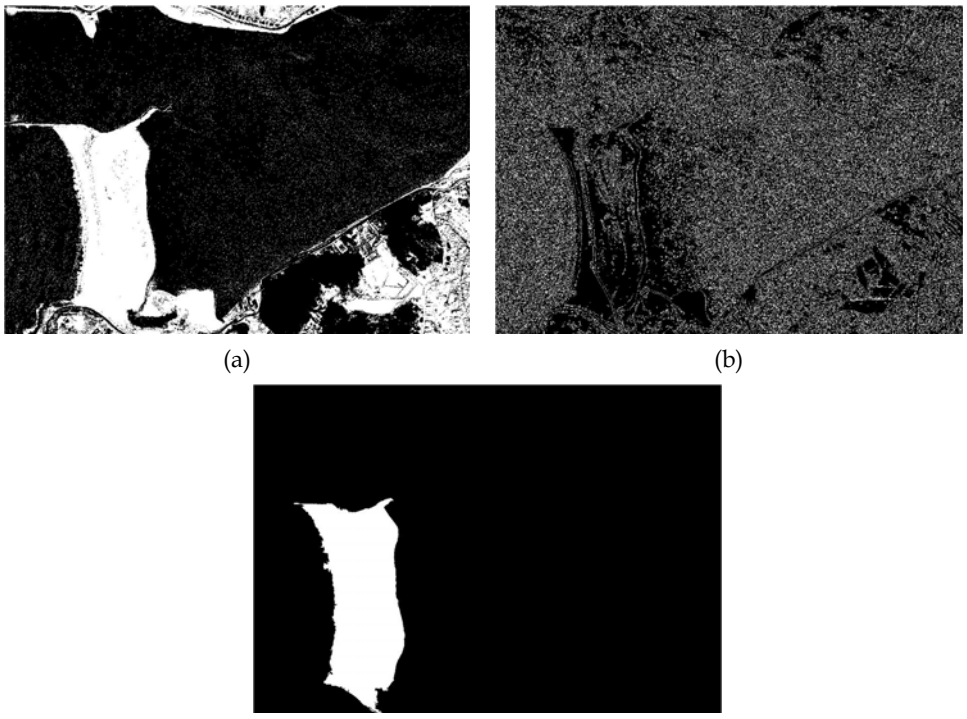

Fig. 7. (a) Global thresholding of the image in Fig. 6a through the Otsu's method; (b) Edges of the image in Fig. 6a obtained through the Canny edge detector; (c) Final extraction of the sand spit in Fig. 6a, through the refinement of the global thresholding in (a) through the edges represented in (b).

2.3.1.2 Edges detection and segmentation refinement

The previous step of global thresholding allows for an initial segmentation of the image. However, the sand spit is frequently still linked to other regions of the image, or to spurious pixels. Therefore, there is the need to perform a refinement on the result of the global thresholding, separating the sand spit from other parts of the image. A refinement of the sand spit delineation is proposed, performed through the application of a binary image obtained from detected edges. Several edge detection methods may be found in the literature, where the Sobel and Canny methods are among the most known (Gonzalez & Woods, 2008). The Sobel is mainly based on computing the partial derivatives $\partial f/\partial x$ and $\partial f/\partial y$ of the image, through the application of filter masks, returning edges at those points where the gradient of the image is maximum. The Canny edge detector is a more complex algorithm, and is based on three basic objectives: low error rate; edge points should be well localized; and single edge point response. Further details of this algorithm may be found in Canny (1986). Based on our experiments, the Canny edge detector, with a standard-deviation of the Gaussian filter equal to 0.5, presented better performance. Therefore, the edges used for further segmentation refinement are obtained in this manner. The edges

computed by the Canny edge detector are then used on a clipping operation of the segmentation previously obtained on global thresholding. In the case that more than one region is produced, and accepting the initial assumption that the considered scene only covers the sand spit and a small neighborhood, the object with largest area is assumed to correspond to the sand spit. As a final segmentation step, the segmentation is improved through a morphological operation, consisting on filling the holes of the segmented object. An application example of the Canny edge detector is provided in Fig. 7b, and the final result is illustrated in Fig. 7c.

2.3.1.3 Evaluation of the global thresholding quality

The global thresholding becomes a simple and useful approach for extracting sand spits, in the case that the histogram of the image presents a bimodal shape. The adequacy of the image to global thresholding using the Otsu's method may be evaluated through the effectiveness metric $\eta(k)$ proposed in (Otsu, 1979), where k is the gray level. The measure $\eta(k)$ is always smooth and unimodal, assumes values between 0 and 1, and the optimal gray level k^* for thresholding the image corresponds to the maximum of $\eta(k)$. The segmentation will be more meaningful as long as $\eta(k^*)$ is near from 1. In Fig. 6 two panchromatic bands of different IKONOS-2 images are illustrated, together with their corresponding histograms and values of $\eta(k^*)$.

An example of 15 combinations of the sand spit area estimation error and their corresponding values of $\eta(k^*)$ is illustrated in Fig. 8. This example also provides an example of a possible criterion to be defined (dashed lines representing an acceptance region), which allows for automatically reject those segmentations which may lead to errors higher than 10%. Further research on this topic may allow for defining objective criteria, in order to evaluate whether an IKONOS-2 image is or not adequate for global thresholding, prior to its application.

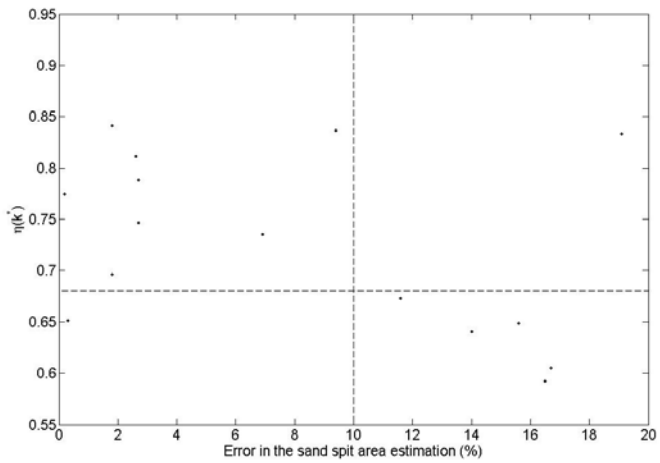

Fig. 8. Effectiveness metric $\eta(k^*)$ of Otsu's method as a function of the error obtained in the sand spit area estimation, considering the four bands of the 6 IKONOS-2 images described in Table 2, which led to sand spit area estimates with an error below 20% (n=15). The dashed lines represent a possible validation threshold based on $\eta(k^*)$ values higher than 0.68, regarding the achievement of errors below 10%.

2.3.2 Multiresolution segmentation

The second approach was based in the multiresolution segmentation method (followed by image-based classification in eCognition® software). The multiresolution segmentation groups areas of similar pixel values into objects. Consequently homogeneous areas result in larger objects, heterogeneous areas in smaller ones. In multiresolution segmentation, the homogeneity criterion is used to determine which heterogeneity attributes of image objects are to be minimized as a result of a segmentation run. Three criteria are used to describe image object heterogeneities: color, smoothness and compactness (Baatz et al., 2001). The smoothness and the compactness criteria are additionally summarized to the shape criterion. The composition of the entire homogeneity criterion based on the specific criteria can easily be defined by assigning weights to each of the specific criteria. The multiresolution segmentation algorithm consecutively merges pixels or existing image objects. Thus it is a bottom-up segmentation algorithm based on a pairwise region merging technique. Multiresolution segmentation is an optimization procedure which, for a given number of image objects, minimizes the average heterogeneity and maximizes their respective homogeneity. Scale parameter determines the average image object size and is an important parameter of this algorithm. The scale parameter is used to determine the upper limit for a permitted change of heterogeneity throughout the segmentation process (Rahman & Saha, 2008). By applying different scale parameter and color/shape combinations, the user is able to create a hierarchical network of image objects (Baatz et al., 2001). After segmentation, all image objects are automatically linked to a network in which each image object knows its neighbors, thus affording important context information for the classification step. In the second step the image segments are classified by generating class hierarchy, which is based on fuzzy logic (Rahman & Saha, 2008).

3. Results and discussion

The previously mentioned image segmentation techniques were applied to extract the Douro river plume and Cabedelo sand spit, both located in the Douro river, city of Porto, Portugal.

3.1 Douro river plume

With respect to the extraction of the Douro river plume, as previously mentioned in 2.1.1, two datasets presenting different characteristics were considered. Between March 2004-2007, two breakwaters were constructed in the Douro river estuary. Therefore, since this is associated to considerable changes in the river estuary dynamics, these two datasets were firstly analysed separately in 3.1.1 and 3.1.2. The comparison of the results obtained with the datasets A and B is given in 3.1.3. The relationship between the river plume size and the water volume, through models previously established in (Teodoro et al., 2009), is explored in 3.1.4.

3.1.1 Dataset A

As previously described in 2.1.1, the dataset A is composed by twenty-one MERIS scenes of the study area, covering 20 months from 2003 to 2005. The methodology used in the determination of the Douro river plume (DRP) size was implemented in Matlab® (Gonzalez et al., 2004). The watershed segmentation was applied using the Sobel filter in the gradient computation before the watershed transform (Gonzalez & Woods, 2008). The region growing segmentation was applied considering as region seeds (S) pixels with DN value of

225, and a threshold (T) of 30. These parameters were obtained on the basis of an iterative process (Teodoro et al., 2009).
After the two segmentation methods described were applied to the MERIS scenes, the small meaningless regions are further excluded, as well as those regions which correspond to rivers and water bodies, leading to the final segmentation result of the river plume. The number of pixels of the remaining regions were summed, resulting in the plume size (Teodoro et al., 2009). An example of a segmented image using both methods is presented in Fig. 4. The values of the plume size obtained through watershed and region-based image segmentation for the 21 MERIS processed scenes, are presented in Table 3.

Date (dd-mm-yyyy)	Plume size		Date (dd-mm-yyyy)	Plume size	
	Watershed	Region-based		Watershed	Region - based
08-03-2003	16 040	25 040	20-01-2004	8 604	13 012
14-05-2003	13 753	36 493	11-02-2004	5 197	15 461
26-05-2003	9 419	14 324	09-04-2004	7 238	23 144
05-06-2003	1 971	7 965	12-04-2004	2 423	15 361
18-06-2003	6 708	33 519	17-05-2004	9 510	17 321
04-07-2003	11 537	13 126	14-08-2004	5 192	7 090
10-07-2003	8 515	14 617	15-09-2004	4 641	16 677
12-09-2003	11 069	21 017	27-09-2004	18 141	24 893
18-09-2003	8 190	13 271	05-11-2004	8 386	15 595
07-10-2003	1 486	11 734	20-01-2005	8 330	16 168
10-12-2003	4 655	9 115			

Table 3. The Douro river plume size values (in number of pixels), obtained through watershed and region-based image segmentation methods, applied to dataset A.

The DRP size obtained through the region-based segmentation (image domain method) led to better results, since its nature allows for a more realistic delineation of the plume (Fig. 4). Since watershed only identifies sharper transitions on the image (it is a feature domain method), the plume is not entirely delineated. The considered segmentation methods retrieved significantly different values, as can be seen in Table 3. For instance, the plume estimation for 07-10-2003 image was 1 486 pixels for the watershed approach and 11 734 pixels for region-based approach. Although the values obtained through these two approaches are linearly related (as previously analyzed in 2.2.2), the differences found between the two segmentation methods are further explored in 3.1.3 and 3.1.4.

3.1.2 Dataset B: one hydrologic year

With the aim of a complete seasonal study of the DRP morphology, one hydrologic year (between August 2008 and October 2009) composed by 107 MERIS scenes (dataset B) were acquired through an ESA funded project. The previous segmentation methods applied to dataset A were firstly applied for the MERIS scenes. In a deeper analysis, it was verified that some MERIS scenes were not adequate for the segmentation purposes. The main reason is related to the presence of clouds or other atmospherics effects that could interfere with the plume extraction. The identification of the images presenting some of these problems was manually performed, resulting in 82 images. According to the work of Teodoro et al., (2009),

the region-based approach is preferable against the watershed segmentation, as the later provides a less accurate delineation of the plume. Therefore, the focus of the segmentation methods applied to dataset B relied on the region growing segmentation.

In the previous analysis, the TSM values in the range 0–50 g/m^3 were rescaled to 8-bit (0-255). However, the region seed (S) and threshold (T) considered in the analysis of dataset A were not adequate for dataset B, due to slight changes on the content of the MERIS scenes. Therefore, in this approach, it was decided to use the TSM concentration values, which required an adaptation of the region seed (S) and threshold (T) considered in the previous work.

The adopted methodology consisted in the development and implementation of an algorithm to automatically select the region seed (S) and the threshold (T) values for each image. In this algorithm two options may be used to select the region seed (S) and the threshold (T) values. The first option consisted in assuming S as the centroid value and T as S/2, whereas the second option is based on assuming S as the mean value of the plume region and T as half the maximum. The second option led to better results, since its nature allows for a more realistic and accurate delineation of the plume (Fig. 9). The average, maximum, minimum and standard deviation values (in number of pixels) of the plume size, obtained through region-based image segmentation method (options 1 and 2) applied to dataset B, are presented in Table 4.

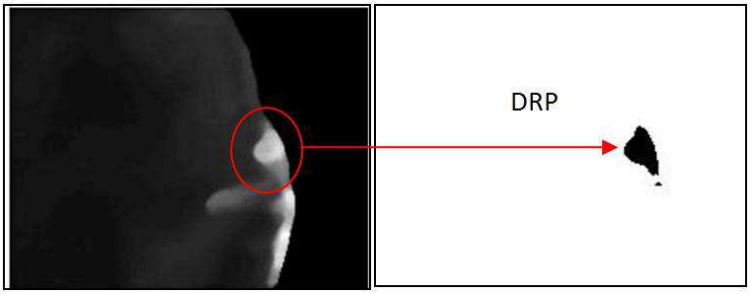

Fig. 9. Example of the segmentation with the developed region growing method (second option).

	Region-based Option 1	Region-based Option 2
Average	391	183
Maximum	997	715
Minimum	27	3
Stdv	250	123

Table 4. Average, maximum, minimum and standard deviation (Stdv) values obtained through the option 1 and option 2 region-based segmentation methods for one hydrologic year of MERIS scenes.

The two segmentation options applied led to different results in terms of the size of the plume. The estimation of the plume size through option 1 led to highest values when compared to the option 2, for all the processed MERIS images.

3.1.3 Comparison of segmentation results obtained from datasets A and B

Despite the slight changes on the selection of the region-growing parameters S and T, it was observed that the river plume size values obtained for dataset B (Table 4) were considerable lower than the values estimated for dataset A scenes (Table 3). This fact can be justified by the construction of two breakwaters between 2004 and 2007, in order to stabilize the Douro river mouth, and with the reduction of water flows and consequently the reduction of the amount of sediments injected into the sea (plume). This may lead in the future to an increase of the sand spit, and deserve further research on this topic.

3.1.4 Relation of river plume size with the water volume

The plume size had been modeled by several authors through satellite data by comparing the quantitative relations between rainstorm and plume size (Nezlin et al., 2005). Others had analyzed the effect of local wind and water discharge on the river plume (Choi & Wilkin, 2007). In this stage of the work, a simple linear regression model of the river plume (RP) on the water volume (Eq. 2) was firstly considered:

$$RP\ (t_i) = a_0 + a_1 * V(t_i) + \varepsilon \tag{2}$$

where ε is the error associated to the proposed model, t_i is the present time of the considered image, a_0 and a_1 are the linear regression coefficients and V is the water volume. The water volume corresponds to the discharged water flow for the last downstream hydroelectric power plant of the Douro river (Crestuma) for each MERIS scene acquisition date. Given the lower river discharges in the summer, a refined analysis was performed considering separately the summer period (comprising 8 and 24 scenes regarding datasets A and B, respectively) associated to lower river discharges, and the rest of the year (the remaining 13 and 58 scenes for datasets A and B, respectively).

With respect to the time period of dataset A, a significant seasonal effect was verified on the relation between the RP and the water volume. Therefore, considering the model presented in Eq. 2 and excluding the summer period, a significant and positive correlation of 0.664 (p−value=0.013) was found between the RP obtained from watershed segmentation and water volume. For region-based segmentation, the correlation coefficient was 0.524 (p−value=0.066) for the same period. No significant correlations (α=5%) were found regarding the summer period. The lack of significant correlation in the summer period may be justified by the lower and time inconstant discharges at Crestuma dam, as illustrated in Fig. 10. The accuracy of this model was quantified by the mean percentage variation (MPV) of each estimated value (e_i, obtained through the model in (2)) to the correspondent computed value (c_i, obtained from segmentation), as presented in Eq. (3):

$$MVP = \frac{1}{N}\sum_{i=1}^{N}\frac{|e_i - c_i|}{c_i} \times 100\% \tag{3}$$

The MPV for watershed was 67.4% and for region-based segmentation was 28.5%. This suggests that the plume size obtained from the region-based segmentation may be more appropriate than the watershed-based segmentation, when modeling the size of the plume as being linearly related to the water volume.

The second proposed model consists in the incorporation of several variables (last available plume, water volume, tide height, and wind speed), presumed to be related to the plume

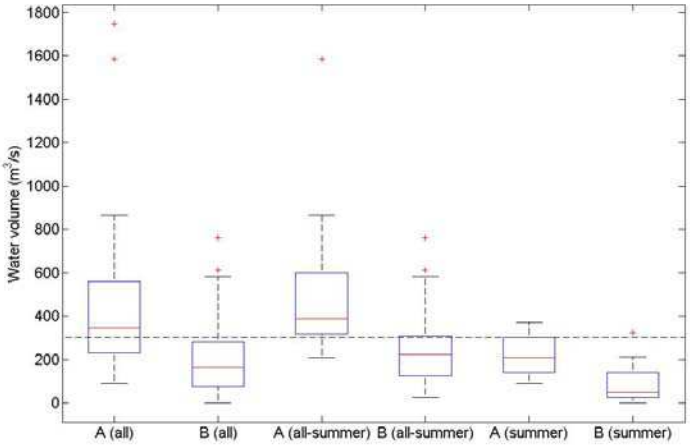

Fig. 10. Water volume (m^3/s) regarding the datasets A and B, considering all dates together ("All"), all year excluding the summer period ("All-Summer") and the Summer period ("Summer").

size. More details about this model may be found in Teodoro et al., (2009). Ignoring the seasonal effects the MPV for watershed was 65.4% and for region-based segmentation was 34.9%. The results of the two models proposed attest the best performance of the region-based segmentation method in the extraction of the Douro river plume size (Teodoro et al., 2009).

A better temporal resolution could increase significantly the performance of the two proposed models, considering and ignoring the seasonal effects. Therefore, the same procedure was applied to the dataset B (one hydrologic year of MERIS scenes). It was verified a significant seasonal effect on the relation between the RP and the water volume. Considering the model presented in Eq. 2 and excluding the summer period, a moderate and positive correlation of 0.45 (p−value=0.019) was found between the RP obtained from region-based segmentation (option 2) and water volume. No significant correlations (α=5%) were found regarding the summer period. Considering all the data, the best result were found for region-based segmentation (option 2) with a positive correlation of 0.37 (p−value=0.003). A more robust model incorporating other variables, as last available plume, water volume, tide height, and wind speed, will be established in order to improve the results. Moreover, a detection of outlying estimations will be performed. An outlier is a value in a dataset which appears to be inconsistent with the remainder of that set of data.

The plume derived from MERIS data represents river Douro plume only when the river flow exceeds a certain threshold. During low discharge, the remotely sensed plume results from other factors, namely, the flow of small rivers, the flow from a big wastewater treatment plant discharge near the river mouth and sediment resuspension resulting from waves, tides, and currents. The threshold between the river flow producing plume and the flow when the plume cannot be estimated from MERIS scenes is about 300 or 500 m^3/s (Teodoro et al., 2009). As illustrated in Fig. 10, the water volumes for the time period of dataset are mostly below 300 m^3/s. Therefore, this explains why lower correlation coefficient values were found for dataset B. Nevertheless, the segmentation approach applied in this work seems to be a valid method to estimate the plume size. The second

option of the proposed region-based method (option 2) appears to be the more accurate alternative.

3.2 Cabedelo sand spit

The segmentation approaches previously mentioned in section 2.3 were applied to 6 IKONOS-2 images (Table 2), and the results are provided in 3.2.1 and 3.2.2. Some experiments considering local filtering methods are addressed in 3.2.3. The evaluation of the performance of global thresholding and multiresolution approaches are given in 3.2.4.

3.2.1 Global thresholding refined by detected edges

As previously mentioned in 2.3, the first segmentation approach mainly consists on histogram thresholding of the original IKONOS-2 image through the Otsu method, followed by a boundary refinement through detected edges. The area estimated for the sand spit through this approach is given in Table 5, regarding the 6 IKONOS-2 images mentioned in Table 2. With respect to the image from 03-06-2004, as already illustrated in Fig. 6, the panchromatic band is not the most suitable band to perform the segmentation. Therefore, the NIR band was used for this image. The disadvantage of using the NIR band instead of the panchromatic band is its lower spatial resolution, which leads to less accurate results, as will be further addressed in 3.2.4.

Date (dd-mm-yyyy)	Area (m^2)			
	2.3.1	2.3.2	Manual reference	DGPS reference
24-12-2001	188 123	198 000	191 056	n.a.
03-06-2004*	260 448	282 000	275 761	265 200
31-07-2004	258 973	250 000	260 095	259 864
03-06-2005	207 214	212 000	212 819	222 636
18-09-2005	229 186	223 000	228 092	228 688
06-06-2007	256 747	261 000	267 208	225 237

* The NIR band was considered instead of the panchromatic band.

Table 5. Sand spit area (m^2) estimated through the segmentation approaches described in 2.3.1 and 2.3.2, applied to the panchromatic bands of the IKONOS-2 images. The last two columns correspond to the reference areas manually obtained (on a GIS environment) and by DGPS field surveys. Further details regarding the reference areas may be found in 3.2.4.

Although the Otsu's method presents a good performance in several cases at the initial stage of global thresholding, it sometimes presents questionable thresholds. In the example provided in Fig. 6, it appears that the most adequate threshold should be slightly shifted. Therefore, other segmentation approaches based on the delineation of the modes in the histogram will deserve further research in the future.

3.2.2 Multiresolution segmentation

In the multiresolution segmentation method, the parameters used for the IKONOS-2 images were (10, 0.5, 0.5, 0.5, 0.5) for (scale, color, shape, smoothness, compactness), respectively. As already mentioned in 2.3.2, after segmentation, all image objects are classified by generating

class hierarchy, based on fuzzy logic (Wang, 1990). The accuracy assessment of the classification process was performed analyzing the confusion matrix (overall accuracy- OA) and Kappa statistics (Smits et al., 1999; Stehman, 1996). The Kappa gives a measure that indicates if the confusion matrix is significantly different from a random result. The performance of the classification of the object-based method was evaluated through the error matrix based on the TTA Mask (Training or Test Areas). The OA varied between 96% (24-12-2001) and 100% (03-06-2005). The Kappa statistics varies between 0.92 and 1.0, for the same image dates. These values demonstrate the good performance of the segmentation and classification methods applied. An example of a sand spit extraction through this approach is illustrated in Fig. 11. The sand spit areas obtained through this segmentation method (described in 2.3) are provided in Table 5.

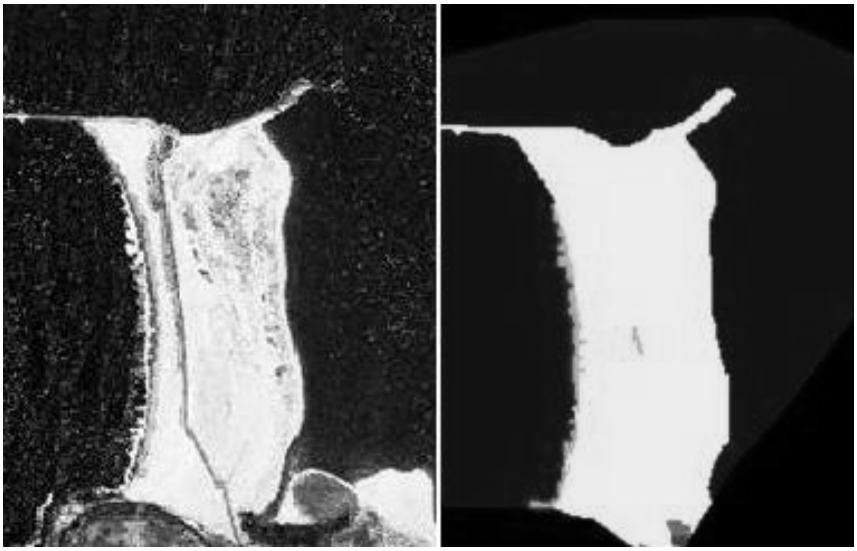

Fig. 11. An original IKONOS-2 image of June 2005 (left) and the sand spit extraction with multiresolution segmentation method - object based classification (right).

3.2.3 Local filtering methods

Other segmentation methods based on local filtering could have been used, such as entropy filtering, range filtering or standard deviation filtering. However, these methods decrease the contrast between the sand spit and the remaining parts of the image, leading to some linkage of the sand spit to other regions of the image. The segmentation of the images produced by entropy, standard deviation and range filtering was also tested, applying the Otsu's method to the filtered images. However, these filtering procedures lead to a lack of accuracy in the sand spit delineation, since it smoothes the transition from sand spit to water, and consequently introducing a connection between the sand spit and water in posterior segmentation. Taking this into account, an edge sensitive version of the low-pass Wiener filtering was also tested, aiming to achieve a more uniform sand spit for later segmentation. However, this also presented considerably lower performance than the proposed global thresholding, followed by refinement through detected edges.

3.2.4 Evaluation of the methods performance

In order to evaluate the performance of the two segmentation methods, used in the estimation of the sand spit area, two sets of reference values were used (Table 5). The first was based on a manual digitalization on a GIS environment of the sand spit on the IKONOS-2 image, followed by the computation of the resultant area. The second approach was based on regular trimesteral surveys conducted since 2002 through Diferencial Global Positioning System (DGPS) processing techniques (Baptista et al., 2008). According to Baptista et al., (2008), the ground point positioning of the sand spit boundary was done through a system comprising two kinematic antennas installed on an articulate arm fixed to a four-wheel motor quad. Because the positioning precision of the kinematic DGPS processing techniques around 0.02 and 0.04 m in planimmetric and altimetric measurements respectively, the overall precision of the determined ground point coordinates were near these values with this DGPS system (Baptista et al., 2008). The values were later processed in a GIS environment and linearly interpolated for different tide levels (z=0, z=1 and z=2 m). These values were used to estimate the correspondent sand spit area, for each analyzed IKONOS-2 image. It is important to refer that the DGPS values do not correspond to the IKONOS-2 acquisition date, but to the closest date (the maximum diference is about 45 days). The reference results obtained through this second approach are given in Table 5. Although a field survey would be the most accurate reference to evaluate the performance of the segmentation methods, the time difference between the field survey and the IKONOS-2 acquisition date for some images was considerably high. This justifies some differences observed in Table 5 between the manual and DGPS reference values.

The average and standard-deviation of the errors (in %), regarding the two segmentation methods described in 2.3.1 and 2.3.2, considering the manual and DGPS reference values are provided in Table 6. It can be observed that the proposed unsupervised segmentation method, based on global thresholding refined through detected edges, presented slightly better results than the multiresolution segmentation, with a clear advantage of a considerable faster performance, beyond requiring a small human intervention.

	Manual reference		DGPS reference	
	Average	Stdv	Average	Stdv
2.3.1	2.4	2.0	4.2	5.0
2.3.2	2.5	1.2	6.7	5.3

Table 6. Average and standard-deviation (Stdv) of the errors (in %), regarding the two segmentation methods described in 2.3.1 and 2.3.2, considering the manual and DGPS reference values (further details in 3.2.4).

In the analysis of the effectiveness metric of the Otsu's method, as a function of the error in the sand spit area estimation, a sketch of a possible threshold of acceptance was illustrated in Fig. 8. However, in the presence of larger datasets, it may become possible to define objective criteria of the appropriateness in using the proposed segmentation methodology. Such criteria may correspond to simple linear discriminants, or to other more complex nonlinear classification approaches, combining information of more than one spectral band.

4. Conclusions

A water body and a sand spit do not present a similar topographic boundary. Therefore, the extraction of a river plume and the extraction of a sand feature from a water environment are different in terms of the segmentation techniques employed. With this work, we have showed that the same segmentation techniques could not be applied directly in both cases.
The reduction of the river sediment supply may be one of the main causes of the erosion process that has been affecting the Portuguese Northwest coast. The Douro river is one of the major sources of beach sediments of the Portuguese Northwest coast. Therefore, the estimation of the river plume size from satellite images is an aspect of crucial importance, since there is no alternative for performing in situ measurements. The applied segmentation methods allowed for estimating the plume size. The plume size obtained through the region-based segmentation led to better results, since its nature allows for a more realistic delineation of the plume.
The reduction of the plume size is probably related to reduction of water flows and consequently the decreasing of river sediment supply. Associated to the breakwaters construction are the changes in the Cadedelo sand spit dynamics. From a regional point of view, this research allows for obtaining data in a simple way, currently nonexistent for the Cabedelo sand spit. Furthermore, it provides significant contributions to evaluate the behaviour of Douro river mouth breakwaters, related with coastal defence and sand spit stabilization, offering an effective and accurate methodology for monitoring the sand spit size. Moreover, it is a valid alternative for the delineation of sand spits, which allows for avoiding expensive DGPS field campaigns.
The use of different satellite data (MERIS products calibrated for TSM concentration and IKONOS raw data) was also a challenge. The considered satellite data showed to be adequate for the established purposes. The medium spatial resolution of MERIS data is enough to estimate the river plume size. Moreover, the high temporal resolution of MERIS data seems to be essential in monitoring the river plume, subject to rapid changes due to extreme situations (e.g. precipitation, floods). The high spatial resolution of IKONOS-2 data also seems to be a crucial factor in the sand spit area estimation.
The proposed unsupervised segmentation strategy for the extraction of the sand spit, presented slightly better performance than the multiresolution segmentation. Moreover, it presents the advantage of being a fast procedure and with a high potential for a fully automation. This would allow for a more consistent analysis of the sand spit behavior and evolution across the time. This approach has also the advantage of avoiding in situ surveys, and allows for assessment of historical records through archived satellite data. Other attributes beyond the area may be easily computed from the result of the sand spit segmentation, allowing for more complex analysis of the sand spit dynamics.
The estuarine environment, particularly the size and temporal and spatial variations of river plumes and sand spits, is an issue of great importance. Furthermore, very few studies have addressed this issue in the past as there are obvious difficulties in establishing an efficient and accurate methodology to extract the features boundaries. This work aspires to cover this gap.

5. Acknowledgements

The authors would like to thank to the European Space Agency (ESA) for providing the MERIS data (Earth Observation Program, Category 1, ID#5899) and the IKONOS images (Earth Observation Program, Category 1, ID# 6495).

The authors would also like to express their acknowledgment to Prof. Veloso-Gomes, Dr. Joaquim Pais-Barbosa and Hélder Almeida for their contributions in some work tasks.

6. References

Baptista, P.; Bastos, L.; Bernardes, C.; Cunha, T. & Dias, J. (2008). Monitoring sandy shores morphologies by DGPS - a practical tool to generate digital elevation models. *Journal of Coastal Research*, Vol. 24, No. 6, pp. 1516-1528.

Baatz, M.; Benz, U.; Dehghani, S.; Heynen, M.; Holtje, A.; Hofmann, P.; Lingenfelder, I.; Mimler, M.; Sohlbach, M.; Weber. M. & Willhauck, G. (2001), eCognition Object-oriented Image Analysis, V.2.2 User Guide. Definiens Imaging, Munchen, Germany.

Bird, E. (2008). *Coastal Geomorphology: An Introduction, second ed.*, John Wiley & Sons, ISBN 978-0470517307, England.

Canny, J. (1986). A computational approach to edge-detection. *IEEE Transactions on Pattern Analysis and Machine Intelligence*, Vol. 8, No. 6, pp. 679-698.

Chen, Q., Yang, X., & Petriu, E. M. (2004). Watershed segmentation for binary images with different distance transforms. *Proceedings of HAVE 2004-IEEE International Workshop on Haptic, Audio and Visual Environments and their Applications*, pp.111-116, Ottawa, Ontario, Canada, Oct. 2004.

Cheng, H. D.; Jiang, X. H.; Sun, Y. & Wang, J. (2001). Color image segmentation: advances and prospects. *Pattern Recognition*, Vol. 34, pp. 2259-2281.

Choi, B. & Wilkin, J. L. (2007). The effect of wind on the dispersal of the Hudson river plume. *J. Phys. Oceanogr.*, Vol. 37, No. 7, pp. 1878–1879.

Daya-Sabar, B. S.; Ghandi, G. & Prakasa-Rao, B. S. (1995). Applications of mathematical morphology in surface water body studies. *International Journal of Remote Sensing*, Vol. 16, pp. 1495-1502.

Doerffer, R.; Sorensen, K. & Aiken, H. J. (1999). MERIS potential for coastal zone applications. *International Journal of Remote Sensing*, Vol. 20, pp. 1809–1818.

Dzwonkowski, B. & Yan, X. H. (2005). Tracking of a Chesapeake Bay estuarine outflow plume with satellite-based ocean color data. *Continental Shelf Research*, Vol. 25, pp. 1942–1958.

European Space Agency. 2007. MERIS Product Handbook, Issue 2.1.

Gonzalez, R. C.; Woods, R. E. & Eddins, S. L. (2004). *Digital Image Processing Using MATLAB*, Prentice Hall, ISBN 978-0130085191, Upper Saddle River, NJ.

Gonzalez, R. C. & Woods, R. E. (2008). *Digital Image Processing*, 3nd ed., Prentice Hall, ISBN 978-0131687288, Upper Saddle River, NJ.

Helder, D.; Coan, M.; Patrick, K. & Gaska, P. (2003). IKONOS geometric characterization. *Remote Sensing of Environment*, Vol. 88, pp. 69–79.

Hojjatoleslami, S. A. & Kittler, J. (1998). Region growing: a new approach. *IEEE Transactions on Image Processing*, Vol. 7, No. 7, pp. 1079-1084.

Lira, J. (2006). Segmentation and morphology of open water bodies from multispectral images. *International Journal of Remote Sensing*, Vol. 27, pp. 4015-4038.

Lira, J.; Morales, A. & Zamora, F. (1997). Study of sediment distribution in the area of the Pánuco river plume by means of remote sensing. *International Journal of Remote Sensing*, Vol. 18, pp. 171-182.

McFeeters, S. K. (1996). The use of the Normalized Difference Water Index (NDWI) in the delineation of open water features. *International Journal of Remote Sensing*, Vol. 7, pp. 1425–1432.

Nezlin, N. P.; DiGiacomo, P. M.; Stein, E. D. & Ackerman, D. (2005). Storm water runoff plumes observed by SeaWiFS radiometer in the Southern California Bight. *Remote Sensing of Environment*, Vol. 98, pp. 494-510.

Otero, M. P. & Siegel, D. A. (2004). Spatial and temporal characteristics of sediment plumes and phytoplankton blooms in the Santa Barbara Channel. *Deep-Sea Research II*, Vol. 51, pp. 1129–1149.

Otsu, N. (1979). A threshold selection method from gray-level histogram. *IEEE Trans. Syst. Man Cybern.*, Vol. 9, pp. 62-66.

Pal, N. R. & Pal, S. K. (1993). A review on image segmentation techniques. *Pattern Recognition*. Vol. 26, No. 9, pp 1277-1294.

Portela, L. I. (2008). Sediment transport and morphodynamics of the Douro River estuary. *Geo-Marine Letters,* Vol. 28, pp. 77-86.

Rahman, M. R. & Saha, S. K. (2008). Multi-resolution segmentation for object-based classification and accuracy assessment of land use/land cover classification using remotely sensed data, *Journal of the Indian Society of Remote Sensing*, Vol. 36, No. 2, pp. 189-201.

Schiller, H. & Doerffer, R. (2005). Improved determination of coastal water constituent concentrations from MERIS data. *IEEE Transactions on Geoscience and Remote Sensing*, Vol. 43, No. 7, pp. 1585–1591.

Smits, P. C.; Dellepiane, S. G. & Schowengerdt, R. A. (1999). Quality assessment of image classification algorithms for land-cover mapping: a review and a proposal for a cost-based approach. *International Journal of Remote Sensing*, Vol. 20, No. 8, pp. 1461-1486.

Stehman, S. V. (1996). Estimating the Kappa coefficient and its variance under stratified random sampling. *Photogrammetric Engineering and Remote Sensing*, Vol. 62, pp. 401-407.

Soh, L. K. & Tsatsoulis, C. (1999). Segmentation of Satellite Imagery of Natural Scenes Using Data Mining. *IEEE Transactions on Geoscience and Remote Sensing*, Vol. 37, No. 2, pp. 1086-1099.

Teodoro, A.; Gonçalves, H.; Veloso-Gomes, F. & Gonçalves, J. A. (2008). Estimation of the Douro River plume dimension based on image segmentation of MERIS scenes. *Proceedings of SPIE, Remote Sensing for Agriculture, Ecosystems, and Hydrology X,* Vol. 7104, pp. , Cardiff, UK, September 2008, Christopher M. U. Neale; Manfred Owe; Guido D'Urso, Editors, 71040F.

Teodoro, A.; Gonçalves, H.; Veloso-Gomes, F. & Gonçalves, J. A. (2009). Modelling of the Douro river plume size, obtained through image segmentation of MERIS data. *IEEE Geoscience and Remote Sensing Letters*, Vol. 6, No. 1, pp. 87-91.

Tremeau, A. & Bolel, N. (1997). A region growing and merging algorithm to color segmentation. *Pattern Recognition*, Vol. 30, No. 7,pp. 1191-1203.

Valente, A. S. & Silva, J. C. B. (2009). On the observability of the fortnightly cycle of the Tagus estuary turbid plume using MODIS ocean colour images. *Journal of Marine Systems*, Vol. 75, pp. 131-137.

Vincent, L. & Soille, P. (1991). Watershed in Digital Spaces: An Efficient Algorithm Based on Immersion Simulations. *IEEE Transactions on Pattern Analysis and Machine Intelligence*, Vol. 13, pp. 583-598.

Wang, F. (1990). Fuzzy supervised classification of remote sensing images. *IEEE Transactions on Geoscience and Remote Sensing*, Vol. 28, No. 2, pp. 194-201.

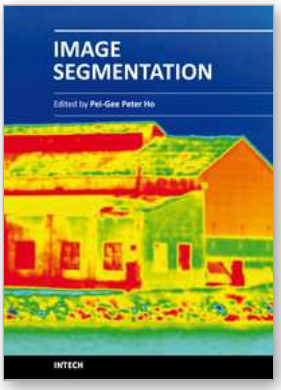

Image Segmentation
Edited by Dr. Pei-Gee Ho

ISBN 978-953-307-228-9
Hard cover, 538 pages
Publisher InTech
Published online 19, April, 2011
Published in print edition April, 2011

It was estimated that 80% of the information received by human is visual. Image processing is evolving fast and continually. During the past 10 years, there has been a significant research increase in image segmentation. To study a specific object in an image, its boundary can be highlighted by an image segmentation procedure. The objective of the image segmentation is to simplify the representation of pictures into meaningful information by partitioning into image regions. Image segmentation is a technique to locate certain objects or boundaries within an image. There are many algorithms and techniques have been developed to solve image segmentation problems, the research topics in this book such as level set, active contour, AR time series image modeling, Support Vector Machines, Pixon based image segmentations, region similarity metric based technique, statistical ANN and JSEG algorithm were written in details. This book brings together many different aspects of the current research on several fields associated to digital image segmentation. Four parts allowed gathering the 27 chapters around the following topics: Survey of Image Segmentation Algorithms, Image Segmentation methods, Image Segmentation Applications and Hardware Implementation. The readers will find the contents in this book enjoyable and get many helpful ideas and overviews on their own study.

How to reference
In order to correctly reference this scholarly work, feel free to copy and paste the following:

Ana Teodoro and Hernâni Gonçalves (2011). Extraction of Estuarine/Coastal Environmental Bodies from Satellite Data through Image Segmentation Techniques, Image Segmentation, Dr. Pei-Gee Ho (Ed.), ISBN: 978-953-307-228-9, InTech, Available from: http://www.intechopen.com/books/image-segmentation/extraction-of-estuarine-coastal-environmental-bodies-from-satellite-data-through-image-segmentation-

INTECH
open science | open minds

InTech Europe
University Campus STeP Ri
Slavka Krautzeka 83/A
51000 Rijeka, Croatia
Phone: +385 (51) 770 447
Fax: +385 (51) 686 166
www.intechopen.com

InTech China
Unit 405, Office Block, Hotel Equatorial Shanghai
No.65, Yan An Road (West), Shanghai, 200040, China
中国上海市延安西路65号上海国际贵都大饭店办公楼405单元
Phone: +86-21-62489820
Fax: +86-21-62489821